멤브레인(Membrane Journal)
Vol. 30 No. 6 December, 2020, 420-432

Print ISSN: 1226-0088
Online ISSN: 2288-7253
DOI: https://doi.org/10.14579/MEMBRANE_JOURNAL.2020.30.6.420

(PIM-*co*-Ellagic Acid)-기반의 이산화탄소 분리막의 개발

호세인 이크발*,**・허스너 아스몰*,**・김 동 영*,**・김 태 현*,**,†

*인천대학교 화학과, **인천대학교 기초과학연구소

(2020년 11월 13일 접수, 2020년 12월 9일 수정, 2020년 12월 10일 채택)

(PIM-*co*-Ellagic Acid)-based Copolymer Membranes for High Performance CO_2 Separation

Iqubal Hossain*,, Asmaul Husna*,**, Dongyoung Kim*,**, and Tae-Hyun Kim*,**,†**

*Organic Material Synthesis Laboratory, Department of Chemistry, Incheon National University, Incheon 22012, Korea
**Research Institute of Basic Sciences, Incheon National University, 119 Academy-ro, Yeonsu-gu, Incheon, 22012, Korea

(Received November 13, 2020, Revised December 9, 2020, Accepted December 10, 2020)

요 약: (PIM-1)과 ellagic acid로 만든 랜덤형 공중합체가 간단한 방법으로 합성되었으며, 이산화탄소 분리막에 대한 적용 가능성에 대해서 연구하였다. 이 공중합체의 경우 PIM (polymers with intrinsic microporosity) 고분자의 미세 기공 구조에 기인한 높은 기체 투과도와 평면 구조와 친수성을 갖는 ellagic acid에 기인한 높은 이산화탄소에 대한 선택성에 의해 우수한 이산화탄소 기체 분리 성능을 나타내었다. 즉, 이산화탄소에 대한 투과도 4516 Barrer와 CO_2/N_2 (> 23~26) 및 CO_2/CH_4 (> 18~19)의 높은 선택성으로 두 쌍의 가스 혼합물에 대해 Robeson 상한(2008)을 초과한 결과를 나타내었다. 이와 같이 PIM-1에 평면구조를 갖는 ellagic acid을 혼입하면 PIM-1의 꼬인 구조를 방해하여 기체 투과성을 향상 시킬 뿐만 아니라 공중합체의 강성과 극성이 증가하여 N_2 및 CH_4에 대한 CO_2의 선택성을 증가시키는 결과를 확인하였다.

Abstract: Random copolymers made of both 'polymer of intrinsic microporosity (PIM-1)' and Ellagic acid were prepared for the first time by a facile one-step polycondensation reaction. By combining the highly porous and contorted structure of PIM (polymers with intrinsic microporosity) and flat-type hydrophilic ellagic acid, the membranes obtained from these random copolymers [(PIM-co-EA)-x] showed high CO_2 permeability (> 4516 Barrer) with high CO_2/N_2 (> 23~26) and CO_2/CH_4 (> 18~19) selectivity, that surpassed the Robeson upper bound (2008) for both pairs of the gas mixture. Incorporation of flat-type ellagic acid into the PIM-1 not only enhances the gas permeability by disturbing the kinked structure of PIM-1 but also increases the selectivity of CO_2 over N_2 and CH_4, due to an increase of rigidity and polarity in the resultant copolymer membranes.

Keywords: *CO_2 separation, random copolymer, ellagic acid, PIM-polymer, gas permeability-selectivity*

1. Introduction

Polymer membrane-based CO_2 separation has attracted significant interest due to its easy processability, low energy consumption, low capital and maintenance cost, compact modulus, and environmental-friendliness over other separation techniques, including cryogenic distillation, amine scrubbing, and pressure swing adsorption[1-3]. Various types of polymer materials have been developed for the CO_2 separation, such as low-quality natural gas, flue gas, and syngas[3-9].

The key parameters used to address the gas separation properties of specific membrane materials are their permeability (P) and selectivity (α), where permeability is a product of diffusivity (D) and solubility (S) coefficients (i.e. $P = D \times S$) and ideal selectivity ($\alpha_{A/B}$)

†Corresponding author(e-mail: tkim@inu.ac.kr, http://orcid.org/0000-0002-1654-3785)

is the ratio of permeability between two single gases ($\alpha_{A/B} = P_A/P_B$). The desired membrane material for gas separation in industrial applications must have both high permeability and high selectivity. Unfortunately, as high permeable polymers are generally less selective and vice versa, pure polymeric membranes inevitably suffer from an undesirable trade-off between gas permeability and selectivity that results from its 'Robeson upper-bound relationship'[10-13].

Various types of commercial polymers have been used for the membrane-based gas separation application, including Cellulose acetate (CA), Pebax polydimethylsiloxane (PDMS), and polyimides (Matrimid) [1-5]. However, most of these polymers do not satisfy the industrial requirements of high CO_2/light gas selectivity (30~50 for CO_2/N_2 separation, and 20~30 for CO_2/CH_4 separation are required) and high CO_2 permeance (> 1000 GPU and > 100 GPU for flue gas and natural gas separation, respectively, are required)[14]. Therefore, the design of a polymer membrane with high permeability and selectivity has become the goal of researchers in this field.

Polymers of intrinsic microporosity (PIMs) have attracted much interest as a novel polymeric membrane material for gas separation in the last decade[15-17]. Having a fused-ring and ladder-type contorted conformation with sites of contortion, the unique structure of PIMs interrupts the packing of polymer chains in the solid-state, causing high free volume and high surface area[18-21]. The corresponding film fabricated from the PIMs (e.g., PIM-1, PIM-7, PIM-PI-1, PIM-PI-8, PIM-Trip. etc.) displays an excellent gas separation performance towards condensable gas (e.g., CO_2) (originated from intrinsic micro-porosity) that surpasses Robeson's upper bounds[3,15-22].

However, the selectivity of CO_2 over other non-polar gases (e.g., N_2 and CH_4) still moderate for the PIMs, which should be improved to obtain highly pure gas from the gas mixture. Moreover, physical aging originated from chain rearrangement and the non-equilibrium state is a major limitation of PIM-based membranes, with implications for their utility in long term applications[5,23]. Several attempts have been made to mitigate this undesirable phenomenon by increasing polymer chain rigidity or by conducting inter-chain cross-linking[23-28]. PIM-1, the first representative polymer with intrinsic microporosity (PIM) having spiro-carbon and CO_2 selective nitrile group was first prepared by Mckeown, and has been upgraded by changing its structure, introducing crosslinking or copolymerization to further increase the gas separation performance[14-20,24-26]. However, the crosslinking of PIM-1 produces several additional limitations, such as a decrease in free volume, reduction of polymer processability, and sacrifice of nitriles, which are key to increasing free volume, selective solubility, and the strength of intermolecular forces because of their lateral position[24-26]. Therefore, the introduction of new monomeric units to the polymer backbone in the form of copolymer structures could be an effective way to increase the rigidity of the polymer chain.

Ellagic acid (EA) is a naturally occurring substance that contains polyphenol chemical moiety with rigid- and flat-molecular structure and is found in many fruits and vegetables, including pomegranate, strawberries, raspberries, blackberries, cherries, grapes, guava, and walnuts[29-33]. Although EA is widely known as an antioxidant, antiproliferative, inflammatory, anticarcinogenic, and inhibitor of chemically induced cancer[32], its four 4-OH groups are strongly nucleophilic towards the electrophilic substance, as are several of its lactone rings, which represent the polar nature of EA[29]. An enhancement of the polarity in the polymer segment (as co-monomer of building block) typically enhances the selectivity of CO_2 over non-polar gases (e.g. N_2 and CH_4) because the polymers containing polar group interact with CO_2, and hence dissolve CO_2[34]. Besides, the flat and rigid nature of EA is expected to affect the kink structure of the PIM-1 chain, which can further modify the overall separation performances of the resultant copolymer membrane. Therefore, EA could be an effective comonomer with the 5,5',6,6'-Tetrahydroxy-3,3,3',3'-tetramethyl-1,10-spirobisindane (THSB), the basic spiro structure of PIM-1, to prepare a PIM-based

copolymer for membrane CO_2 separation with enhanced rigidity and selectivity.

We report herein a straightforward one-step preparation of random-type copolymers, combining THSB and EA monomers with tetrafluorophthalonitrile (TFN) through polycondensation reaction, designated as [(PIM-co-EA)-x], with a 0 to 5 mol% loading of EA. To the best of our knowledge, this is the first example of using an EA-based copolymer membrane for gas separation application. The copolymers were characterized by ^{1}HNMR, IR, and TGA, and the morphology and CO_2 gas separation properties of the corresponding membranes were investigated.

2. Experiment

2.1. Materials

5,5',6,6'-Tetrahydroxy-3,3,3',3'-tetramethyl-1,10-spirobisindane (THSB, 3, 97%) was obtained from Alfa Aesar (Seoul, Korea). Ellagic acid (EA, 4) was purchased from Tokyo Chemical Industry (TCI) Co. Ltd. (Seoul, Korea) and was used as obtained. Tetrafluorophthalonitrile (TFN, 2), acetic anhydride, toluene, and triethylamine were obtained from Sigma Aldrich (Yongin, Korea). Methanol, chloroform, dimethylformamide, potassium carbonate, and potassium hydroxide were purchased from DaeJung Chemicals & Metals Co. Ltd. (Shiheung, Korea).

2.2. Synthesis of [(PIM-co-EA)-x] copolymers (1) with different compositions

The copolymers (PIM-co-EA)-x (1) with different loading (x) of EA (4) were synthesized following a published procedure[15]. For (PIM-co-EA)-1 (1 mol% of EA), 500 mg (2.5 mmol) of TFN (2) (previously purified by recrystallization from hot acetone), 842 mg (2.473 mmol) of THSB (3) (recrystallized from methanol), 8 mg (0.027 mmol) of EA (pre-dissolved in 1.5 mL of dry NMP), and 2.85 g of anhydrous K_2CO_3 were stirred under an atmosphere of dry N_2 at 65°C for 3 days in 20 mL of 'dry' dimethylformamide (DMF). Upon cooling, the crude product was separated by precipitation in methanol and washed with water followed by methanol to remove any impurities or unreacted monomers. After drying at 80°C overnight in a vacuum oven, the solid was dissolved in 20 mL of chloroform and precipitated into 400 mL of methanol. The reprecipitation procedure was performed three times, and the copolymer was finally collected as bright yellow granules. Yield (92%); δ_H (400 MHz, $CDCl_3$); 7.5 (0.02 H, s, Ar*H*), 6.8 (2H, s, Ar*H*), 6.4 (2H, s, Ar*H*), 2.3~2.1 (4H, dd, -C*H*$_2$-), 1.3 (12 H, br, -C*H*$_3$-), ATR-IR (cm^{-1}) 3058 (Aromatic C-H stretching), 2958, 2924 & 2864 (C-H stretching), 168, 1446 (aromatic C=C stretching), 1210, 1192, 1108,1009 (Ar-O-Ar).

The copolymer (PIM-co-EA)-5 was prepared by following the same procedure using different mole ratio (1 : 0.05) of THSB and EA. Yield (89%); δ_H (400 MHz, $CDCl_3$); 7.5 (0.1 H, s, Ar*H*), 6.8 (2H, s, Ar*H*), 6.4 (2H, s, Ar*H*), 2.3~2.1 (4H, dd, -C*H*$_2$-), 1.3 (12 H, br, -C*H*$_3$-), ATR-IR (cm^{-1}) 3058 (Aromatic C-H stretching), 2958, 2924 & 2864 (C-H stretching), 168, 1446 (aromatic C=C stretching), 1210, 1192, 1108,1009 (Ar-O-Ar).

PIM-1 was also prepared by following the same procedure without using EA monomer. Yield (93%); δ_H (400 MHz, $CDCl_3$); 6.8 (2H, s, Ar*H*), 6.4 (2H, s, Ar*H*), 2.3~2.1 (4H, dd, -C*H*$_2$-), 1.3 (12H, br, -C*H*$_3$-), ATR-IR (cm^{-1}) 3058 (Aromatic C-H stretching), 2958, 2924 & 2864 (C-H stretching), 168, 1446 (aromatic C=C stretching), 1210, 1192, 1108, 1009 (Ar-O-Ar).

2.3. Membrane preparation

Each polymer membrane was prepared using a solution (~3 wt% in $CHCl_3$) casting method into a flat-bottomed glass dish, followed by slow evaporation of the solvent at ambient temperature as follows. The corresponding copolymers with different compositions (1) were dissolved in $CHCl_3$ (~3% w/v, g/mL), stirred at room temperature overnight, and then filtered. Each polymer solution was carefully poured into a glass dish, covered with aluminum foil that had been punctured with small holes, and allowed to undergo solvent evaporation at r.t for 3 days. It was then placed in an oven, and the solvent was completely dried at 70°C for

24 hours. The dry membranes were obtained, cooled to room temperature, peeled away from the glass plate, dried again at 70°C in an oven for 24 hours, and finally stored at ambient temperature. The thickness of all the membranes was controlled to fall within the range of 35 to 45 μm.

2.3. Characterization and measurements

The ^{1}H NMR spectra were obtained on an Agilent 400-MR (400 MHz) instrument, using d_6-DMSO or $CDCl_3$ as a reference or an internal deuterium lock. The attenuated total reflection Fourier transform infrared (ATR-FTIR) spectra were recorded using a Bruker Vertex 80v Hyperion 2000 ATR-FTIR spectrometer. The densities of the membranes (gcm^{-3}) were determined experimentally using a top-loading electronic Mettler Toledo balance (XP205, Mettler-Toledo, Switzerland) coupled with a density kit based on Archimedes' principle. The samples were weighed in air and a known-density liquid, that is, high purity heptane. The measurement was performed at room temperature by the buoyancy method, and the density was calculated as follows:

$$\rho_{polymer} = \frac{W_0}{W_0 - W_1} \times \rho_{liq}$$

where W_0 and W_1 are the membrane weights in air and heptane, respectively, and ρ_{liq} is the density of the liquid. The thermal stability of the membranes was analyzed by thermogravimetric analysis (TGA) measurements conducted on a Shimadzu TGA-2950 instrument at a heating rate of 10°C min^{-1} under a nitrogen flow. The X-ray diffraction patterns of the membranes were measured using a Rigaku DMAX-2200H diffractometer operated at a scanning rate of 4° min^{-1} in a 2θ range from 5° to 30° with Cu Kα1 X-ray radiation (λ = 0.1540598). The *d*-spacings were calculated using Bragg's law ($d = \lambda/2\sin\theta$).

The pure gas permeation performance of copolymer membranes was measured using a high-vacuum time lag measurement unit based on the constant-volume/variable-pressure method. All the gas separation experiments were conducted at a feed pressure of 1 atm and a feed temperature of 30°C. Before the gas permeation measurements, both the feed and the permeate sides were thoroughly evacuated until the readout showed zero values to remove any residual gases. The downstream volume was calibrated using a Kapton membrane and was found to be 55.57 cm^3. The upstream and downstream pressures were measured using a Baraton transducer (MKS, model no. 626B02TBE) with a full scale of 100000 and ~0 Torr, respectively. The pressure rise versus time transient of the permeate side, equipped with a pressure transducer, was recorded and passed to a desktop computer through a shield data cable. The permeability coefficient of each gas was determined from the linear slope of the downstream pressure rise versus time plot (dp/dt) according to the following equation:

$$P = \frac{273}{76} \times \frac{V_1}{ATp_0} \times \frac{dp}{dt} \quad (1)$$

where, P is the permeability coefficient expressed in Barrer (1 Barrer = 10^{-10} cm^3 (STP) cm cm^2 s^{-1} $cmHg^{-1}$); V (cm^3) is the downstream volume; l (cm) is the thickness of the membrane; A (cm^2) is the effective area of the membrane; T (K) is the temperature of measurement; p_0 (Torr) is the pressure of the feed gas in the upstream chamber and dp/dt is the rate of the pressure rise under the steady-state. The gas permeation tests of each gas were repeated more than three times, and the standard deviation from the mean values of permeabilities was within ca. 3%. Sample to sample reproducibility was found to be high and within 3%. The effective membrane areas where gas permeates were 2.54 cm^2. The ideal permselectivity, $\alpha_{A/B}$, of the membrane for a pair of gases (A and B) was calculated from the ratios of the individual gas permeability coefficients, and can be described as shown in Eqn (2):

$$\alpha_{A/B} = \frac{P_A}{P_B} \quad (2)$$

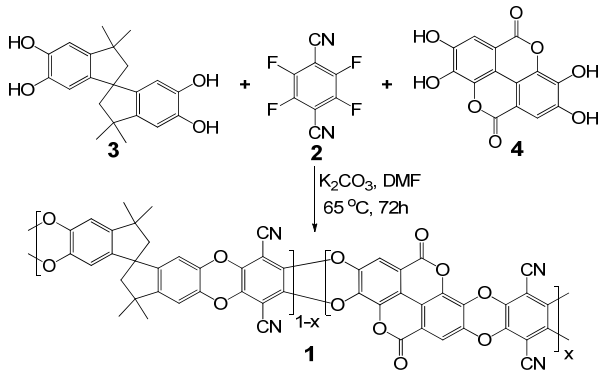

Scheme 1. Synthesis of [(PIM-co-EA)-x] copolymers copolymers (1) with different loading (x) of EA.

The diffusivity and solubility coefficients were obtained from the time-lag value according to the following Eqn (3):

$$D = \frac{l^2}{6\theta} \tag{3}$$

where, D (cm^2s^{-1}) is the diffusivity coefficient, l is the membrane thickness (cm) and θ is the time lag (s), obtained from the intercept of the linear steady-state part of downstream pressure rise versus time plot. Solubility, S, was calculated from eqn (4) with permeability and diffusivity obtained from Eqn (1) and (3).

$$S = \frac{P}{D} \tag{4}$$

3. Results and Discussion

3.1. Synthesis and characterization of the [(PIM-co-EA)-x] copolymers (1)

Following the reported method, the random-type copolymers composed of both PIM-1 and EA-TFN were prepared by a polycondensation reaction between two tetrahydroxy (3 and 4) and a tetrafluoride (2) monomer (Scheme 1)[15]. The copolymers were designated as [(PIM-co-EA)-x], where x represents the mol% of ellagic acid loading compared to total tetrahydroxy monomer (i.e., THSB + ellagic acid). These were termed (PIM-co-EA)-1 and (PIM-co-EA)-5, for 1 mol% and 5 mol% EA incorporated copolymer, respectively. The PIM-1 polymer (i.e., does not contain any ellagic acid monomer) was also prepared for comparison. However, copolymers containing more than 5 mol% ellagic acid loading showed granules that did not provide self-standing membranes, probably due to the crystallinity originated from EA.

The structure and composition of PIM-1 and the copolymers, (PIM-co-EA)-1 and (PIM-co-EA)-5, were determined from ^{1}HNMR analysis by comparing the integral ratio between two comonomers; for example, the peak integration corresponding to the phenyl proton of ellagic acid (H_7) was compared with the peak integration of the spirobisindane-based phenyl protons ($H_{1,2}$) and was found to be 1 : 0.01 compared to 1 : 0.05 (Fig. 1). However, the peak position of other aromatic and aliphatic peaks remained unchanged in both copolymers.

The structures of [(PIM-co-EA)-x] copolymers (1) were further analyzed by ATR-IR spectroscopy (Fig. 2). It was found that aromatic the C-H and C=O stretching peak at 3058 cm^{-1} and 1717 were enhanced slightly for copolymers compared to PIM-1. All other peaks of PIM-1 for aliphatic C-H, C≡N, C=C and Ar-O-Ar remained unchanged for all polymers (Fig. 2). This result can be explained by the significantly smaller presence of EA and similar functional groups in the copolymers' structure compared to the PIM-1 structure.

The structure of the copolymers was further characterized by TGA analysis, which will be detailed in the following section.

3.2. Preparation of the [(PIM-co-EA)-x] copolymer membranes

The [(PIM-co-EA)-x] copolymer membranes with two different compositions, denoted as (PIM-co-EA)-1 and (PIM-co-EA)-5, and the pure PIM-1 were prepared using the solution-casting method with $CHCl_3$ (as a membrane casting solvent) solution of each polymer to give flexible membranes with a thickness ranging from 35 to 45 μm (Fig. 3). All three membranes were readily soluble in organic solvents such as $CHCl_3$, $CHCl_2$, and THF, but were sparingly soluble in DMF and

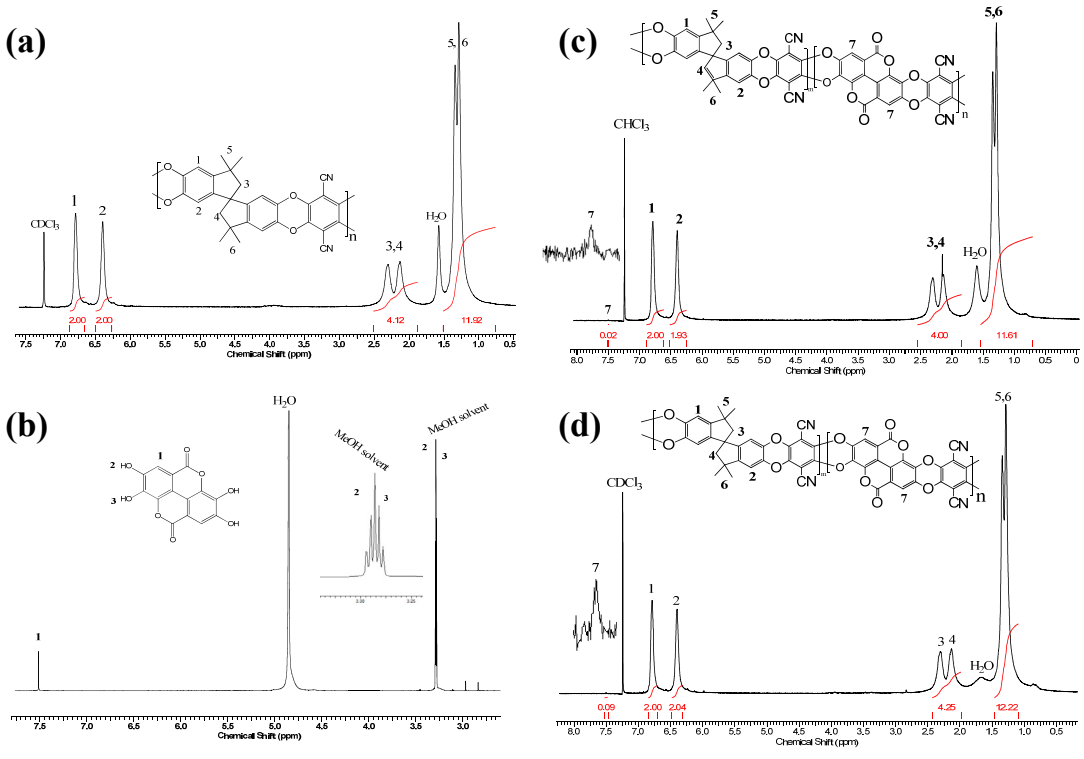

Fig. 1. ^{1}HNMR spectra for (a) PIM-1 homopolymer; (b) Ellagic acid monomer, (c) (PIM-co-EA)-1 copolymer, and (d) (PIM-co-EA)-5 copolymer.

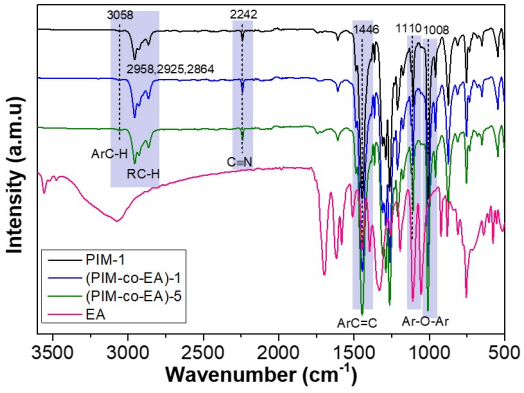

Fig. 2. ATR-FTIR spectra of the [(PIM-co-EA)-x] copolymers with loading of EA.

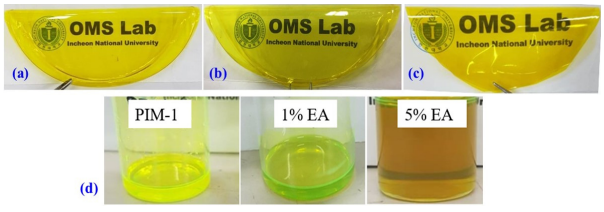

Fig. 3. Pictures of the copolymer membranes: (a) PIM-1, (b) (PIM-co-EA)-1, (c) (PIM-co-EA)-5, and (d) 2 wt.% solution of the above copolymers showing different colors at the solution state.

DMSO. It was noticed that the color of the copolymer solutions was different (pale yellow) compare to the original fluorescence active in the PIM-1 polymer solution (Fig. 3d). This is an indirect indication of the presence of EA in the copolymer structure. However, the color of the dried membrane did not show any noticeable differences between various compositions.

3.3. Physical and thermal properties

It was found that the density of the copolymer membranes was first decreased at 1 mol% EA loading for the (PIM-co-EA)-1 membrane, followed by a slight increase at 5 mol% loading for the (PIM-co-EA)-5 membrane. The reduction of density might be aroused by the prohibition of the regular orientation of the PIM-1 polymer by the flat ellagic acid comonomer. In contrast, a slight increase in density at a high loading of EA may be originated from both close packing of

Table 1. Physical Properties of the[(PIM-co-EA)-x] Copolymer Membranes

Membrane code	Thermal decomposition (°C)		ρ (g · cm^{-3})	*d*-spacing (Å)
	$T_{max}1$	$T_{max}1$		
PIM-1	-	511	1.11	14.94, 7.62, 5.0
(PIM-co-EA)-1	420	507	1.07	11.62, 7.37, 4.92
(PIM-co-EA)-5	463	502	1.09	15.80, 7.43, 4.90

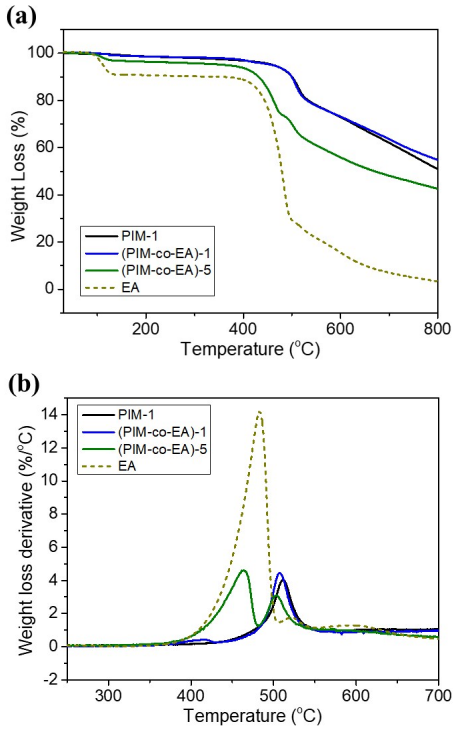

Fig. 4. (a) TGA curve of the copolymer membranes, and (b) First order derivative curve of the corresponding membranes.

rigid EA segment at its high loading and high density of EA (1.67 g · cm^{-3}).

The thermal properties of the [(PIM-co-EA)-x] copolymer membranes were investigated by TGA and were compared with the PIM-1 polymer membrane (Table 1 and Fig. 4). As shown in Fig. 4, the PIM-1 showed high thermal stability up to > 500°C (with a T_{max} ~511°C) without any weight loss. In contrast, the EA monomer displayed a two-step weight loss: the first degradation occurred around 110°C, which is attributed to the evaporation of bound water bonded through the hydrogen bond, followed by the second weight loss onset at around 400°C (T_{max} ~483°C) due to the backbone degradation of EA[33]. Fig. 4a and the derivative curve in Fig. 4b clearly show that both copolymers had a two-step principle degradation with a maximum weight loss temperature, T_{max}, at 420°C and 507°C for (PIM-co-EA)-1 and at 463°C and 502°C for (PIM-co-EA)-5, respectively, with an initial weight loss for bound water evaporation. This is experimental evidence of the presence of EA in the copolymer structure, and it indicates that the amount of weight loss increases with the increase of EA content in the copolymer. However, overall thermal stability was suitable for the applications requiring high-temperature CO_2 separation of our [(PIM-co-EA)-x] copolymer membranes (Fig. 4 and Table 1).

3.4. Morphological analysis by XRD

The morphologies of the pure PIM-1 and (PIM-co-EA)-x copolymer membranes were investigated using wide-angle X-ray diffraction (WAXD) to determine the crystallinity and intermolecular chain distance of the polymers.

Fig. 5 shows the WAXD data of the PIM-1, (PIM-co-EA)-1, and (PIM-co-EA)-5 polymer membranes. Similar wide distribution peaks were observed with a slightly different peak position for all copolymer membranes, except a highly intense and broadly distributed new peak around 7° (2θ) for the (PIM-co-EA)-1 copolymer membrane. This broad distribution curve indicates the amorphous nature of all copolymer membranes. The polymer-polymer intersegmental distance (or d-spacing) was further estimated using Bragg's law, $d = \lambda / 2 \sin \theta$ (λ: the wavelength of 1.54 Å; θ: the scattering angle) (Table 1).

Table 2. Gas Permeability[a] and Selectivity of the (PIM-co-EA)-x Copolymer Membranes at 30°C and 1 Atm Pressure. Gas Separation Data from Various Reports are also Presented for Comparison

Membrane code	Permeability			Ideal selectivity	
	P_{CO2}	P_{N2}	P_{CH4}	$\alpha_{CO2/N2}$	$\alpha_{CO2/CH4}$
PIM-1	3912	168.9	216.6	23.2	18.1
(PIM-co-EA)-1	5483	240.8	288.5	22.8	19.0
(PIM-co-EA)-5	4516	179.3	234.8	25.2	19.2
PIM-1[b]	3934	269	366	14.6	11.0
PIM-1[c]	3496	238	360	14.7	9.7
PIM-1[d]	2300	92	125	25	18.4
PIM-1[e]	3364	182	218	18.5	15.4
PIM-1[f]	3799	228	310	16.6	12.2
PIM-1[g]	4390	180	310	24.4	13.9
PIM-1[h]	6500	340	430	19.0	15.1

[a] Permeability in Barrer, where 1 Barrer = 10^{-10}[cm^3 (STP)cm][cm^{-2} s^{-1} cm^{-1} Hg^{-1}]; [b] Ref. [24], [c] Ref. [16], [d] Ref. [15], [e] Ref. [35], [f] Ref. [36], [g] Ref. [37] and [h] Ref. [38].

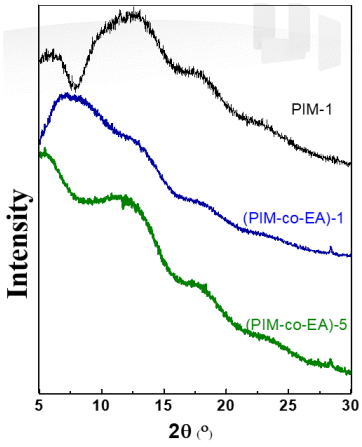

Fig. 5. Wide-angle XRD diagrams of the [(PIM-co-EA)-x] copolymers with different loading of ellagic acid.

It was showed that the peaks arise due to the fact that the loosely packed and closely packed chain distance at 7.6 Å and 5.0 Å for PIM-1 was shifted to the slightly lower d-spacing at around 7.4 Å and 4.9 Å for the copolymers (PIM-co-EA)-x. This may be originated due to the incorporation of flat-type EA monomer into the kinked PIM-1 polymer. Surprisingly, a highly intense and broadly distributed new peak was observed at around 11.6 Å for the (PIM-co-Ea)-1 copolymer membrane, showing the imperfect packing of polymer-polymer chains. This indicates that the flat-type EA structure can disturb the regular kinked orientation of the PIM-1 chain and enable the creation of a more loosely packed structure. However, that new peak did not appear at a high loading of EA [i.e., (PIM-co-EA)-5]. Instead, the peaks due to the distance between kinked C-to-C distance was originated in a manner similar to the PIM-1 polymer. The exact explanation of this behavior is beyond the scope of the present work; we leave it to our future studies. Finally, the presence of EA in the copolymer structure was further confirmed by a crystalline peak, which appeared at a diffraction angle of (2θ) 28°.

3.5. Gas separation performance of the copolymer membranes

The pure gas (N_2, CH_4, and CO_2) permeabilities of the PIM-1 and [(PIM-co-EA)-x] copolymer membranes were determined at 30°C and 1 atm pressure using the constant-volume/variable-pressure method and their ideal selectivities (i.e. $\alpha_{CO2/N2}$ and $\alpha_{CO2/CH4}$) were calculated by dividing the permeability of CO_2 with the permeability of N_2 and CH_4 (Table 2 and Fig. 6). The diffusivities were obtained from the time-lag instrument, and solubilities were calculated using Eqn. 4.

It was shown that all the polymer membranes, in-

Table 3. Gas Diffusivity[a] and Solubility[b] of the (PIM-co-EA)-x Copolymer Membranes at 30°C and 1 Atm Pressure

Membrane Code	Diffusivity[a]			Solubility[b]		
	D_{CO2}	D_{N2}	D_{CH4}	S_{CO2}	S_{N2}	S_{CH4}
PIM-1	23.5	28.7	8.4	166.5	5.9	25.8
(PIM-1-EA)-1	32.6	48.4	12.6	168.2	5.0	22.9
(PIM-1-EA)-5	26.8	36.6	10.5	168.5	4.9	22.4

[a] Diffusivity coefficient (10^{-8} cm^2/s), [b] solubility coefficient (10^{-2} cm^3 (STP)/cm^3 cmHg).

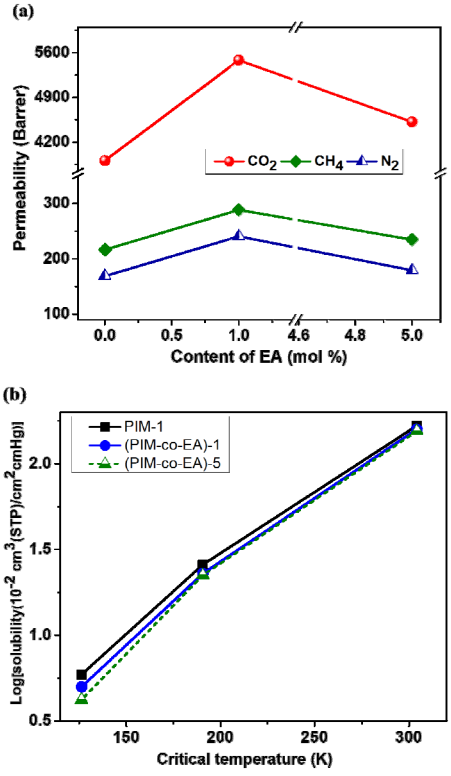

Figure 6. (a) Gas permeability of the [(PIM-co-EA)-x] copolymers with different loading of ellagic acid, and (b) pure gas solubilities of the copolymer membranes as a function of the critical temperature of the corresponding gases.

cluding PIM-1 and both copolymer membranes i.e., (PIM-co-EA)-1 and (PIM-co-EA)-5 exhibited higher CO_2 permeability (> 3912 Barrer) relative to other gases (i.e. N_2 and CH_4): CO_2 >> CH_4 > N_2. This order in permeabilities could be attributed to the combined effect of diffusivity and solubility of the gases. It was noticed that the order of the gas diffusivity (N_2 > CO_2 > CH_4), which is related to the kinetic diameter of the penetrant gases and is inversely proportional to the gas molecule size [CO_2 (3.30 Å) < N_2 (3.64 Å) < CH_4 (3.80 Å)], did not correlate properly with the separation property of individual gases in the present experiment. Instead, the trend of gas permeability is the same as that of the solubility order of the gases: S_{CO2} > S_{CH4} > S_{N2}, which is directly related to the critical temperature, T_c, of the gases [CO_2 (304.2 K) > CH_4 (190.6 K) > N_2 (126.2 K)] (Table 3 and Fig. 6b). In other words, the solubility of the gases determined the order of gas permeability for all membranes because the gases with a higher critical temperature displayed higher solubility coefficients and condensability, and this behavior predominates in the polymer with intrinsic microporosity and hence high interaction with polar gases such as PIM-1.

It is noteworthy that the performance of the pristine PIM-1 membrane is comparable (Table 2) to that of most of the PIM-1 reported in the literature[15,16,24,35-38]. The variation either in permeability or selectivity between the present work and the reported result is acceptable because the gas separation performance of the highly permeable glassy polymer is solely dependent on various parameters, such as the solvent used for membrane casting, the post-treatment of the membrane, the pressure, and the temperature at which the performance analyzed.

When we compared the gas separation properties of the copolymer membranes - i.e., (PIM-co-EA)-1 and (PIM-co-EA)-5 - with the pristine PIM-1 polymer, we observed that the permeability of all the gases for the (PIM-co-EA)-1 copolymer membrane with 1 mol% EA loading was increased compared to the pure PIM-1 membrane (Table 2). For example, the permeability of

CO_2, N_2, and CH_4 were increased by 40.2, 42.5, and 33.2% respectively. In contrast, the 5 mol% EA loaded copolymer membrane, (PIM-co-EA)-5, showed a reduced permeability to all gases compared to (PIM-co-EA)-1 by 21.1, 25.5, and 18.6% for CO_2, N_2, and CH_4 gases, respectively (Table 2). However, the permeabilities of CO_2, N_2, and CH_4 gases for the (PIM-co-EA)-5 copolymer membrane were still 15.4, 6.2, and 8.4%, respectively, higher than that of the pristine PIM-1 membrane.

To explain the behavior of gas permeability, we first compared the solubility coefficients of the various membranes and observed that the CO_2 solubility of the copolymer membranes did not change significantly, though it followed a slight increasing order: PIM-1 < (PIM-co-EA)-1 < (PIM-co-EA)-5. In contrast, the solubility order of non-polar gas was reversed: PIM-1 > (PIM-co-EA)-1 > (PIM-co-EA)-5. None of these followed the order of gas permeability when we compared different copolymer compositions. The order of CO_2-solubility can be explained by the hydrophilic nature of ellagic acid that helps to enhance the solubility of polar CO_2 gas as opposed to the non-polar N_2 and CH_4 gases, and thus it also helps to enhance the selectivity of CO_2 over the other gases.

It was noticed that the key factor that affects the increment of permeability by EA loading is diffusivity, which increased similarly but to a greater extent, like that of the permeability of all gases. For example, the diffusivities of 1 mol% EA loaded copolymer [(PIM-co-EA)-1] membrane to CO_2, N_2, and CH_4 gases were increased by 46.8, 68.6, and 50.0% respectively, compared to the PIM-1 membrane, followed by a slight reduction by 15.7, 12.2, and 16.7% respectively, to the 5 mol% EA loaded copolymer (PIM-co-EA)-5 membrane compare to the (PIM-co-EA)-1 (Table 3). However, the diffusivities of CO_2, N_2, and CH_4 gases for the (PIM-co-EA)-5 copolymer membrane were still 23.8, 48.1, and 25.0%, respectively, higher than that of pristine PIM-1 membrane (Table 3). This trend of increasing diffusivity (hence permeability) at 1 mol% loading, to all gases, may be attributed to the increment of the free-volume in the [(PIM-co-EA)-1] copolymer structure due to disturbance of the regular kinked orientation of PIM-1 chain at low loading (1 mol%), as evidenced by the XRD measurement. The reduction of diffusivity at high (5 mol%) loading, an indication of the free volume reduction by other means, can be explained by the close packing of the polymer chain in a region with a flat EA-rich polymer chain, as evidenced by the XRD analysis.

The selectivity of the present PIM-1 membrane for CO_2/N_2 and CO_2/CH_4 gas pairs were 23.2 and 18.1, respectively, which is very similar to the study carried out by P.M. Budd *et al.*[15] but higher than that of the majority of the studies reported in the literature [16,24,35-38]. It was also observed that the CO_2/N_2 selectivity of the 1 mol% EA loaded membrane [(PIM-co-EA)-1] was somewhat similar to that of the PIM-1 membrane (Table 2), but it was increased at the 5 mol% EA loaded copolymer [(PIM-co-EA)-5] membrane. Moreover, the CO_2/CH_4 selectivity showed a greater gradual increase with the increase of EA loading compared to that of the PIM-1 membrane. This increment in selectivity for both pairs of gases was expected because the EA-moiety showed an increase, compared to the PIM-1 structure, in the rigidity and CO_2-philicity of the copolymer due to the combination of its flat-type molecular structure and polarity.

3.6. Permeability vs. selectivity

The trade-off between permeability (P) and ideal selectivity (α) is a common phenomenon for most polymer membrane-based gas separation strategies (i.e., higher permeability is obtained at the cost of reduced selectivity and vice versa). The CO_2 permeability versus the CO_2/N_2 (Fig. 7a) and CO_2/CH_4 (Fig. 7b) selectivity values of the newly developed [(PIM-co-EA)-x] membranes were then placed at the upper bound of the Robeson plots, and compared with the reported values obtained from the typical PIM-1[1,4,15,16,24,35-38], together with PIM-PI-type homo- and copolymers[1,3,4,28].

The results showed that our copolymer [(PIM-co-EA)-x] outperformed most of the PIM-1 and PIM-PI-

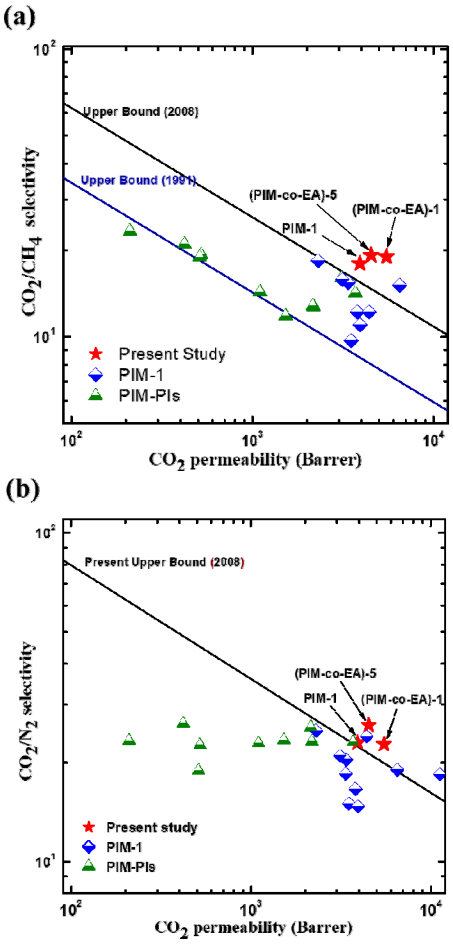

Fig. 7. 'Robeson upper bound' plots comparing (a) the CO_2/N_2 and (b) the CO_2/CH_4 separation performance capabilities of the copolymer membranes with other reported PIM-1 and PIM-1 based copolymer membranes; data taken from [1,3,4,10,11,15,16,24,28,35-38].

based homo and copolymers (Fig. 7). Furthermore, the trade-off results of the [(PIM-co-EA)-x] copolymers crossed the upper bound line of 2008 for CO_2/N_2 and CO_2/CH_4 gas pairs (Fig. 7). The performance indicates that our copolymer could be an excellent candidate for CO_2 separation applications.

4. Conclusions

Random-type [(PIM-co-EA)-x] copolymers with two different compositions (1 mol% and 5 mol% EA loading) were synthesized for the first time using a facile one-step polycondensation reaction. By combining the highly porous and contorted structure of PIM with the flat-type EA structure with rigidity and polarity, the membranes obtained from these [(PIM-co-EA)-x] copolymers showed excellent CO_2 permeability (> 4583 and 5483 Barrer), with high CO_2/N_2 (over 23) and CO_2/CH_4 (over 19) selectivity that surpassed the Robeson upper bound (2008) for both pairs of gases. The excellent separation performance of the newly developed copolymer membranes makes them competitive polymer materials for CO_2 separation applications.

Acknowledgements

This work was supported by Basic Science Research Program through the National Research Foundation of Korea (NRF) funded by Ministry of Education (NRF-2017R1A6A1A06015181).

Reference

1. S. Wang, X. Li, H. Wu, Z. Tian, Q. Xin, G. He, D. Peng, S. Chen, Y. Yin, Z. Jiang, and M. D. Guiver, "Advances in high permeability polymer-based membrane materials for CO_2 separations", *Energy Environ. Sci.*, **9**, 1863 (2016).
2. A. B. Rao and E. S. Rubin, "A technical, economic, and environmental assessment of amine-based CO_2 capture technology for power plant greenhouse gas control", *Environ. Sci. Technol.*, **36**, 4467 (2002).
3. I. Hossain, S. Y. Nam, C. Rizzuto, G. Barbieri, E. Tocci, and T.-H. Kim, "PIM-polyimide multiblock copolymer-based membranes with enhanced CO_2 separation performances", *J. Memb. Sci.*, **574**, 270 (2019).
4. N. Du, H. B. Park, M. M. Dal-Cin, and M. D. Guiver, "Advances in high permeability polymeric membrane materials for CO_2 separations", *Energy Environ. Sci.*, **5**, 7306 (2012).
5. I. Hossain, D. Kim, A. Z. Al Munsur, J. M. Roh, H. B. Park, and T.-H. Kim, "PEG/PPG-PDMS-based cross-linked copolymer membranes prepared by ROMP and *in situ* membrane casting for CO_2 sep-

aration: An approach to endow rubbery materials with properties of rigid polymers", *ACS Appl. Mater. Interfaces*, **12**, 27286 (2020).
6. H. You, I. Hossain, and T.-H. Kim, "Piperazinium-mediated crosslinked polyimide-polydimethylsiloxane (PI-PDMS) copolymer membranes: The effect of PDMS content on CO_2 separation", *RSC Adv.*, **8**, 1328 (2018).
7. D. Kim, I. Hossain, Y. Kim, O. Choi, and T.-H. Kim, "PEG/PPG-PDMS-adamantane-based crosslinked terpolymer using the ROMP technique to prepare a highly permeable and CO_2-selective polymer membrane", *Polymers*, **12**, 1 (2020).
8. I. Hossain, A. Z. Al Munsur, O. Choi, and T.-H. Kim, "Bisimidazolium PEG-mediated crosslinked 6FDA-durene polyimide membranes for CO_2 separation", *Sep. Purif. Technol.*, **224**, 180 (2019).
9. J. H. Park, D. J. Kim, and S. Y. Nam, "Characterization and preparation of PEG-polyimide copolymer asymmetric flat sheet membranes for carbon dioxide separation", *Membr. J.*, **25**, 547 (2015).
10. L. M. Robeson, "Correlation of separation factor versus permeability for polymeric membranes", *J. Memb. Sci.*, **62**, 165 (1991).
11. L. M. Robeson, "The upper bound revisited", *J. Memb. Sci.*, **320**, 390 (2008).
12. S. J. Moon, H. J. Min, N. U. Kim, and J. H. Kim, "Fabrication of polymeric blend membranes using PBEM-POEM comb copolymer and poly(ethylene glycol) for CO_2 capture", *Membr. J.*, **29**, 223 (2019).
13. S. Y. Yoo and H. B. Park, "Membrane-based direct air capture technologies", *Membr. J.*, **30**, 173 (2020).
14. P. M. Budd, K. J. Msayib, C. E. Tattershall, B. S. Ghanem, K. J. Reynolds, N. B. McKeown, and D. Fritsch, "Gas separation membranes from polymers of intrinsic microporosity", *J. Memb. Sci.*, **251**, 263 (2005).
15. N. Prasetya, N. F. Himma, P. D. Sutrisna, I G. Wenten, and B. P. Ladewig, "A review on emerging organic-containing microporous material membranes for carbon capture and separation", *Chem. Eng. J.*, **391**, 123575 (2020).
16. C. L. Staiger, S. J. Pas, A. J. Hill, and C. J. Cornelius, "Gas separation, free volume distribution, and physical aging of a highly microporous spirobisindane polymer", *Chem. Mater.*, **20**, 2606 (2008).
17. N. Du, H. B. Park, G. P. Robertson, M. M. Dal-Cin, T. Visser, L. Scoles, and M. D. Guiver, "Polymer nanosieve membranes for CO_2-capture applications", *Nat. Mater.*, **10**, 372 (2011).
18. N. B. McKeown, "Polymers of intrinsic microporosity", *ISRN Mater. Sci.*, **2012**, 1 (2012).
19. N. B. McKeown and P. M. Budd, "Exploitation of intrinsic microporosity in polymer-based materials", *Macromolecules*, **43**, 5163 (2010).
20. C. Ma and J. J. Urban, "Polymers of intrinsic microporosity (PIMs) gas separation membranes: A mini review", *Proc. Nat. Res. Soc.*, **2**, 02002 (2018).
21. W. H. Lee, J. G. Seong, X. Hu, and Y. M. Lee, "Recent progress in microporous polymers from thermally rearranged polymers and polymers of intrinsic microporosity for membrane gas separation: Pushing performance limits and revisiting trade-off lines", *J. Polym. Sci.*, **1** (2020).
22. B. Comesaña-Gándara, J. Chen, C. G. Bezzu, M. Carta, I. Rose, M. C. Ferrari, E. Esposito, A. Fuoco, J. C. Jansen, and N. B. McKeown, "Redefining the Robeson upper bounds for CO_2/CH_4 and CO_2/N_2 separations using a series of ultrapermeable benzotriptycene-based polymers of intrinsic microporosity", *Energy Environ. Sci.*, **12**, 2733 (2019).
23. X. Chen, Z. Zhang, L. Wu, X. Liu, S. Xu, J.E. Efome, X. Zhang, and N. Li, "Polymers of intrinsic microporosity having bulky substitutes and cross-linking for gas separation membranes", *ACS Appl. Polym. Mater.*, **2**, 987 (2020).
24. J. W. Jeon, D. G. Kim, E. H. Sohn, Y. Yoo, Y. S. Kim, B. G. Kim, and J. C. Lee, "Highly carboxylate-functionalized polymers of intrinsic microporosity for CO_2-selective polymer membranes", *Macromolecules*, **50**, 8019 (2017).
25. S. Neumann, G. Bengtson, D. Meis, and V. Filiz, "Thermal cross linking of novel azide modified polymers of intrinsic microporosity-effect of dis-

tribution and the gas separation performance", *Polymers*, **11**, 1241 (2019).
26. N. Du, M. M. Dal-Cin, G. P. Robertson, and M. D. Guiver, "Decarboxylation-induced cross-linking of polymers of intrinsic microporosity (PIMs) for membrane gas separation", *Macromolecules*, **45**, 5134 (2012).
27. K. Halder, S. Neumann, G. Bengtson, M. M. Khan, V. Filiz, and V. Abetz, "Polymers of intrinsic microporosity postmodified by vinyl groups for membrane applications", *Macromolecules*, **51**, 7309 (2018).
28. I. Hossain, A. Z. Al Munsur, and T.-H. Kim, "A facile synthesis of (PIM-polyimide)-(6FDA-durene-polyimide) copolymer as novel polymer membranes for CO_2 separation", *Membranes*, **9**, 113 (2019).
29. F. M. Mady and M. A. Shaker, "Enhanced anticancer activity and oral bioavailability of ellagic acid through encapsulation in biodegradable polymeric nanoparticles", *Int. J. Nanomedicine*, **12**, 7405 (2017).
30. E. M. Daniel, A. S. Krupnick, Y. H. Heur, J. A. Blinzler, R. W. Nims, and G. D. Stoner, "Extraction, stability, and quantitation of ellagic acid in various fruits and nuts", *J. Food Compos. Anal.*, **2**, 338 (1989).
31. I. Kang, T. Buckner, N. F. Shay, L. Gu, and S. Chung, "Improvements in metabolic health with consumption of ellagic acid and subsequent conversion into urolithins: Evidence and mechanisms", *Adv. Nutr.*, **7**, 961 (2016).
32. J. L. Maas, G. J. Galletta, and G. D. Stoner, "Ellagic acid, an anticarcinogen in fruits, especially in strawberries: A review", *HortScience.*, **26**, 10 (1991).
33. M. Z. Hussein, S. H. Al Ali, Z. Zainal, and M. N. Hakim, "Development of antiproliferative nanohybrid compound with controlled release property using ellagic acid as the active agent", *Int. J. Nanomedicine*, **6** , 1373 (2011).
34. T. Sakaguchi and T. Hashimoto, "Synthesis of poly (diphenylacetylene)s bearing various polar groups and their gas permeability", *Polym. J.*, **46**, 391 (2014).
35. J. Liu, Y. Xiao, K. S. Liao, and T. S. Chung, "Highly permeable and aging resistant 3D architecture from polymers of intrinsic microporosity incorporated with beta-cyclodextrin", *J. Memb. Sci.*, **523**, 92 (2017).
36. X. M. Wu, Q. G. Zhang, P. J. Lin, Y. Qu, A. M. Zhu, and Q. L. Liu, "Towards enhanced CO_2 selectivity of the PIM-1 membrane by blending with polyethylene glycol", *J. Memb. Sci.*, **493**, 147 (2015).
37. J. Ahn, W. J. Chung, I. Pinnau, J. Song, N. Du, G. P. Robertson, and M. D. Guiver, "Gas transport behavior of mixed-matrix membranes composed of silica nanoparticles in a polymer of intrinsic microporosity (PIM-1)", *J. Memb. Sci.*, **346**, 280 (2010).
38. S. Thomas, I. Pinnau, N. Du, and M. D. Guiver, "Pure- and mixed-gas permeation properties of a microporous spirobisindane-based ladder polymer (PIM-1)", *J. Memb. Sci.*, **333**, 125 (2009).